Journal of Hydrology 640 (2024) 131669

Contents lists available at ScienceDirect

Journal of Hydrology

journal homepage: www.elsevier.com/locate/jhydrol

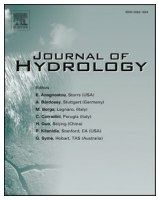

Research papers

Global socioeconomic risk assessment of rainstorms based on different CMIP6 scenarios in the future

Xiufang Zhu [a,b], Mingxiu Tang [a,b,*], Tingting Liu [a,b], Chunhua Guo [a,b]

[a] Key Laboratory of Environmental Change and Natural Disasters, Ministry of Education, Beijing Normal University (BNU), Beijing 100875, PR China
[b] Institute of Remote Sensing Science and Engineering, Faculty of Geographical Science, BNU, Beijing 100875, PR China

ARTICLE INFO

Keywords:
CMIP6
SSPs
Global rainstorm
Socioeconomic risk

ABSTRACT

The extreme weather caused by global warming is increasing day by day. It is of great significance to reasonably assess the risk from extreme precipitation in the world to reduce the losses caused by disasters. Based on the daily precipitation simulation data of 22 global climate models (GCMs) under three scenarios, shared socioeconomic pathways (SSPs) 1–2.6, 2–4.5, and 5–8.5 in the Coupled Model Intercomparison Project Phase 6 (CMIP6), this study calculated three rainstorm indicators (annual rainstorm days, ARDs; annual rainstorm intensity, ARI; and annual rainstorm maximum, ARM), combined them into an index to indicate rainstorm hazard, calculated the socioeconomic exposure index using the projected future population and GDP data of SSP1, SSP2, and SSP3, and finally combined the rainstorm hazard index and socioeconomic exposure index to calculate the socioeconomic risk index of rainstorms. The socioeconomic risks from rainstorms in different periods (1995–2014, 2041–2060, and 2081–2100) were compared at global and continental scales. The main factors that cause the differences in the socioeconomic risks from rainstorms on different continents were explored. The uncertainties of the three rainstorm indicators calculated from the 22 GCMs were analyzed. The main conclusions are as follows: (1) The socioeconomic risk from rainstorms in most regions of the world will increase in the future, with the largest increase in the SSP5-8.5 scenario and the smallest increase in the SSP1-2.6 scenario. Compared with the historical period, the number of grids with increased risk in the mid-term (2041–2060) and long-term (2081–2100) is 97.58% and 97.98% under the SSP5-8.5 scenario, respectively. Under the SSP1-2.6 scenario, the number of grids with increased risk in the mid-term (2041–2060) and long-term (2081–2100) is 89.20% and 86.57%, respectively. (2) Overall, in the two future periods, the least socioeconomic risk from rainstorms is in Europe, and the largest socioeconomic risk from rainstorms is in Asia, especially the southern and southeastern parts of Asia, which have both the highest mean socioeconomic risk and the largest growth of socioeconomic risk. (3) The socioeconomic risk changes of rainstorms in North and South America, Africa, Asia, and Oceania are more closely related to socioeconomic exposure changes, while the socioeconomic risk changes of rainstorms in Europe are more closely related to the three rainstorm indicators. (4) Among the three scenarios, the SSP5-8.5 scenario has the largest uncertainty, and among the three rainstorm indicators, ARDs have the largest uncertainty. The regions with the greatest uncertainty are concentrated in central North America, Central America, central and southern Africa, central South America, eastern Asia, and southern Oceania.

1. Introduction

The Intergovernmental Panel on Climate Change (IPCC) pointed out in the Sixth Assessment Report (AR6) that global warming of 1.5 ℃ and 2 ℃ is expected to be exceeded during the 21st century. Global warming will lead to the continuous strengthening of climate system changes (Zhang et al., 2013), which increases and enlarges the frequency, intensity, and coverage trends of impacts from extreme weather and

Abbreviations: GCM, Global climate models; SSP, Shared socioeconomic pathway; CMIP6, Coupled Model Intercomparison Project Phase 6; ARDs, Annual rainstorm days; ARI, Annual rainstorm intensity; ARM, Annual rainstorm maximum; IPCC, Intergovernmental Panel on Climate Change; AR6, Sixth Assessment Report; GDP, Gross domestic product; H, Rainstorm hazard index; E, Socioeconomic exposure index; NEX-GDDP-CMIP6, NASA Earth Exchange Global Daily Downscaled Projections; NIES, National Institute for Environmental Studies.

* Corresponding author.
E-mail address: 202131051050@mail.bnu.edu.cn (M. Tang).

https://doi.org/10.1016/j.jhydrol.2024.131669
Received 24 January 2024; Received in revised form 7 May 2024; Accepted 29 June 2024
Available online 18 July 2024

climate events in the global scope (Liu et al., 2015; Tang, 2019; Ragettli et al., 2019; AghaKouchak et al., 2020; Zhou et al., 2021), such as extreme high temperature, rainstorms, drought and heatwaves. These extreme events will have serious adverse impacts on the ecological environment, social economy, and human life and health at global and regional scales (Bowles et al., 2014; Liu and Chen, 2021; Zhu et al., 2021), greatly threatening the sustainable development of society and human well-being (Hauer et al., 2021; Tate et al., 2021; Tellman et al., 2021). Therefore, it is of great significance for the formulation of disaster prevention and mitigation policies in various regions of the world to accurately assess the hazards of extreme events and predict population and economic exposure to extreme events under climate change scenarios.

The World Meteorological Organization divides precipitation into seven grades (Tan et al., 2015; World Meteorological Organization, 2012), of which daily precipitation greater than 50 mm is called rainstorm, which is one kind of extreme precipitation. In recent years, research on extreme precipitation has been increasing, significant progress has been made in the analysis of spatial and temporal distribution characteristics, influencing factors, and trends of extreme precipitation (Abdila and Nugroho, 2021; Li et al., 2020; Noor et al., 2019; Uranchimeg et al., 2020; Wang et al., 2017, 2019; Zhang et al., 2021). Besides, extreme precipitation can induce meteorological and geological disasters, such as floods, landslides, and debris flows (Hu et al., 2021; Melillo et al., 2015), which hurt human production and life. Therefore, in the context of intensified climate change, more and more researchers paid attention to the potential impact of future extreme precipitation on human society and the economy (Chen and Sun, 2020; Franzke, 2021; Weaver et al., 2017).

Table 1 summarizes the main research in recent years on the potential socioeconomic impacts of extreme precipitation in future scenarios, particularly the changes in population and gross domestic product (GDP) exposure with changes in extreme precipitation. Some studies have used historical observations and future simulation data of precipitation, population, and GDP to analyze the changes in population and GDP exposure to extreme precipitation on a global or regional scale in a certain period in the future (Chen and Sun, 2021; Liu et al., 2020b; Sun et al., 2021; Tang and Hu, 2022; Xu et al., 2022a). Other studies have calculated and compared the change in the economy and population exposure to extreme precipitation under 1.5 ℃, 2 ℃, and 3 ℃ increasing temperature scenarios based on global climate model (GCM) data (Ayugi et al., 2022; Qin, 2022; Shi et al., 2021; Ta et al., 2022; Zhao et al., 2021). In general, considering the uncertainty of model simulations, existing studies have usually used more than 10 climate datasets simulated by GCMs as input to reduce the uncertainty of single model simulation results. The scenarios used in different studies were different, among which SSP1-2.6, SSP2-4.5, and SSP5-8.5 were the most commonly used climate scenarios. From the perspective of the study area, most studies have focused on local areas. From the perspective of exposure, most studies have only considered population, not GDP, especially in the two global scale studies based on CMIP6 (Table 1). However, the potential adverse impact of rainstorm disaster (risk) is the consequence of the interaction among the hazard of rainstorms, the exposure, and the vulnerability of rainstorm-bearing bodies. According to the disaster risk assessment paradigm of the United Nations Office for Disaster Risk Reduction (UNDRR), the determination of risk can be expressed as the product of hazard, exposure, and vulnerability (United Nations Office for Disaster Risk Reduction, 2019). So far, there is no comprehensive assessment of socioeconomic risk assessment of rainstorms under future climate scenarios. Accurate socioeconomic risk assessment of rainstorms can help people understand the potential adverse effects of rainstorms, identify the hot spots vulnerable to rainstorms, clarify the factors affecting the socioeconomic risks of rainstorms, scientifically plan urban land use, reasonably layout buildings and infrastructure, strengthen the monitoring and management of areas vulnerable to rainstorm, and develop scientific and effective disaster prevention and mitigation measures.

In response to the issues raised in the aforementioned research, based on the daily precipitation simulation data of 22 GCMs under three scenarios, SSP1-2.6, SSP2-4.5, and SSP5-8.5 in CMIP6, this study extracted the annual rainstorm days (ARDs), annual rainstorm intensity (ARI) and annual rainstorm maximum (ARM) and combined these three indicators into an index to indicate rainstorm hazards; calculated the socioeconomic exposure index using future population and GDP data from SSP1, SSP2, and SSP3; and finally assessed and compared the socioeconomic risks of rainstorms in the mid-term (2041–2060) and long-term (2081–2100) on global and continental scales. Compared with previous work, the main novelty of this study lies in three aspects. First, it gives a more comprehensive description of rainstorm risk, integrates population and GDP into the socioeconomic exposure index (*E*), integrates ARDs, ARI, and ARM into the rainstorm hazard index (*H*), and further integrates *E* and *H* into a risk index. Second, it used the future daily precipitation data of 22 GCMs in CMIP6 to calculate the three rainstorm indicators (ARDs, ARI, and ARM) to reduce the uncertainty between models and quantitatively analyzed the uncertainty of the three rainstorm indexes calculated by different models through coefficient of

Table 1
Summary of existing studies regarding the impact of extreme precipitation under future scenarios.

Authors, year		Future scenarios	Models	Hazard indicators	Warming Levels	Exposure	Study area
Liu et al. (2020b)	CMIP5	RCP2.6, RCP4.5, RCP8.5	5	Days of extreme precipitation	—	Population and GDP	Global
Shi et al. (2021)		RCP4.5, RCP8.5	29	Days of extreme precipitation	1.5, 2 ℃	Population and GDP	Global
Zhao et al. (2021)		RCP2.6, RCP4.5, RCP8.5	5	Days of extreme precipitation	1.5, 2, 3 ℃	Population	Region
Sun et al. (2021)	CMIP6	SSP1-2.6, SSP2-4.5, SSP5-8.5	10	Days of daily precipitation amount ≥ 20 mm	—	Population	Region
Chen and Sun. (2021)		SSP1-2.6, SSP2-4.5, SSP3-7.0, SSP5-8.5	23, 25, 21, 25	Days of extreme precipitation	—	Population	Global
Tang and Hu. (2022)		SSP1-2.6, SSP2-4.5, SSP5-8.5	26	Days of extreme precipitation	—	Population	Region
Ayugi et al. (2022)		SSP2-4.5, SSP5-8.5	26	Extremely wet days, duration of dry days	1.5, 2 ℃	Population	Region
Ta et al. (2022)		SSP1-2.6	12	The number of annual extreme precipitation events, the areal coverage of each extreme precipitation event	1.5 ℃	Population and GDP	Region
Xu et al. (2022a)		SSP1-2.6, SSP2-4.5, SSP3-7.0, SSP5-8.5	20	The frequency of dangerous precipitation extremes	—	Population	Region
Qin (2022)		SSP2-4.5	16	Consecutive wet days and consecutive dry days	1.5, 2 ℃	Population	Global

variation. Third, the main factors that cause the changes in the socioeconomic risks of rainstorms on each continent were explored. This study is expected to provide a reference for a more comprehensive and objective understanding of the distribution patterns, changes, influencing factors, and uncertainties of global rainstorm socioeconomic risks and guide us to focus on high-risk areas and high-uncertainty areas.

2. Data and methods

2.1. Data

Compared with CMIP5, CMIP6 has higher data quality and resolution (Du et al., 2022; Xu et al., 2022b; Zhu et al., 2020). This study used 22 GCMs from NASA Earth Exchange Global Daily Downscaled Projections (NEX-GDDP-CMIP6), which were produced using the bias-correction and spatial-disaggregation approach (Thrasher et al., 2022). NEX-GDDP-CMIP6 provides simulated data with a time resolution of 1 day and a spatial resolution of 0.25° under three scenarios (SSP1-2.6, SSP2-4.5, and SSP5-8.5). The details of the GCMs are shown in Table 2. Among the three scenarios used in this study, SSP1-2.6 represents the comprehensive impact of low social vulnerability, low mitigation pressure, and low radiation forcing; SSP2-4.5 is an intermediate path of a combination of moderate development and moderate emission scenarios, which is closer to the current social development status; and SSP5-8.5 is a shared socioeconomic path for human-caused radiation forcing to reach 8.5 W/m^2 in 2100 (O'Neill et al., 2016). During this research, we used two time periods: the mid-term (2041–2060) and long-term (2081–2100).

Future population and GDP datasets were obtained from the National Institute for Environmental Studies (NIES), Japan (Murakami and Yamagata, 2019). These datasets are available every 10 years under the SSP1, SSP2, and SSP3 paths, with a spatial resolution of 0.5 degrees. The downscale approach used in the process of data production assumed that the city population changes over time and that urban areas expand or shrink according to the city population change. The city populations were downscaled into 0.5-degree grids considering the specific characteristics and dynamics of each city including its population change, urban expansion/shrinkage, and auxiliary variables such as road network and land cover. Besides, spatial and socioeconomic interactions among cities were used to accurately estimate the population and GDP at a finer spatial resolution. The downscaling approach utilized a model ensemble technique to estimate the influence of each factor and allows for control over urban shrinkage or dispersion based on the SSPs. The population/GDP average from 2041 to 2060 was used as the social/economic exposure in the mid-term period. The population/GDP average from 2081 to 2100 was used as the social/economic exposure in the long-term period.

Table 2
22 GCMs of CMIP6 used in this study.

Model name	Country	Days/year
ACCESS-CM2	Australia	365/366
ACCESS-ESM1-5	Australia	365/366
BCC-CSM2-MR	China	365
CanESM5	Canada	365
CMCC-CM2-SR5	Italy	365
CMCC-ESM2	Italy	365
EC-Earth3	Ten European countries	365/366
EC-Earth3-Veg-LR	Ten European countries	365/366
GFDL-ESM4	USA	365
INM-CM4-8	Russia	365
INM-CM5-0	Russia	365
IPSL-CM6A-LR	France	365/366
KACE-1–0-G	Korea	360
KIOST-ESM	Korea	365
MIROC6	Japan	365/366
MPI-ESM1-2-HR	Germany	365/366
MPI-ESM1-2-LR	Germany	365/366
MRI-ESM2-0	Japan	365/366
NESM3	China	365/366
NorESM2-LM	Norway	365
NorESM2-MM	Norway	365
TaiESM1	China	365

2.2. Methods

The overall technical flowchart is shown in Fig. 1. It includes 5 main steps: calculating the rainstorm hazard index (H) based on future precipitation data from 22 models under three scenarios (SSP1-2.6, SSP2-4.5, and SSP5-8.5) of NEX-GDDP-CMIP6, calculating the exposure index (E) of rainstorm-bearing bodies based on the future GDP and population data, calculating rainstorm socioeconomic risks based on H and E, calculating the coefficient of variation of rainstorm hazard calculated from different GCM simulation data grid by a grid to assess the uncertainty of different GCM, and analyzing the leading factors causing spatial differences in rainstorm risk changes on each continent based on the geographic detector. The above five steps were carried out in the two future periods (2041–2060 and 2081–2100).

2.2.1. Calculation of the rainstorm hazard index

According to the precipitation classification of the World Meteorological Organization, daily precipitation greater than 50 mm is defined as a rainstorm (Tan et al., 2015). Therefore, this study used 50 mm as the threshold to determine whether there was a rainstorm and calculated the ARDs, ARI, and ARM. ARDs refer to the total number of rainstorm days in a year. ARI refers to the average precipitation of all rainstorm days in a year. ARM refers to the maximum precipitation of all rainstorm days in a year.

We take the calculation of ARDs as an example to introduce the calculation of the three rainstorm indicators in the future. First, for each GCM, we calculated the ARDs according to the daily precipitation prediction data in 2041–2060 and then calculated the mean value of ARDs in 2041–2060. Second, we took the mean ARDs of 22 GCMs in 2041–2060 as ARDs in the mid-term period. Third, the ARDs were normalized between 0 and 1 using the minimum and maximum values.

With the above method, we calculated the standardized values of the three rainstorm indicators (ARDs, ARI, and ARM) in the two future periods (2041–2060 and 2081–2100). Then, for each future period, the mean value of three standardized rainstorm indicators was calculated and taken as the rainstorm hazard index (H).

2.2.2. Calculation of the exposure index of rainstorm-bearing bodies

Similarly, we first calculated the average population from 2041 to 2060, interpolated the average population to a 0.25° resolution through area weight interpolation, and standardized the population to 0–1 using the minimum and maximum values, respectively. Using the same method, we calculated the population and GDP standardized values for the two future periods (2041–2060 and 2081–2100). Then, for each period in the future, we calculated the average of the standardized population and GDP as the exposure index (E).

2.2.3. Calculation of socioeconomic risks

The socioeconomic risk calculation formula is as follows:

$$Risk = \sqrt{H \times E} \quad (1)$$

where H is the rainstorm hazard index; E is the exposure index of the rainstorm-bearing body; and $Risk$ represents the socioeconomic risks caused by rainstorms.

The socioeconomic risks of rainstorms in the historical and future scenarios were calculated by Eq. (1). It should be noted that in the calculation of socioeconomic risks of rainstorms, since no population and GDP datasets under SSP5 path in the dataset obtained from the National Institute for Environmental Studies (NIES), Japan, the hazard

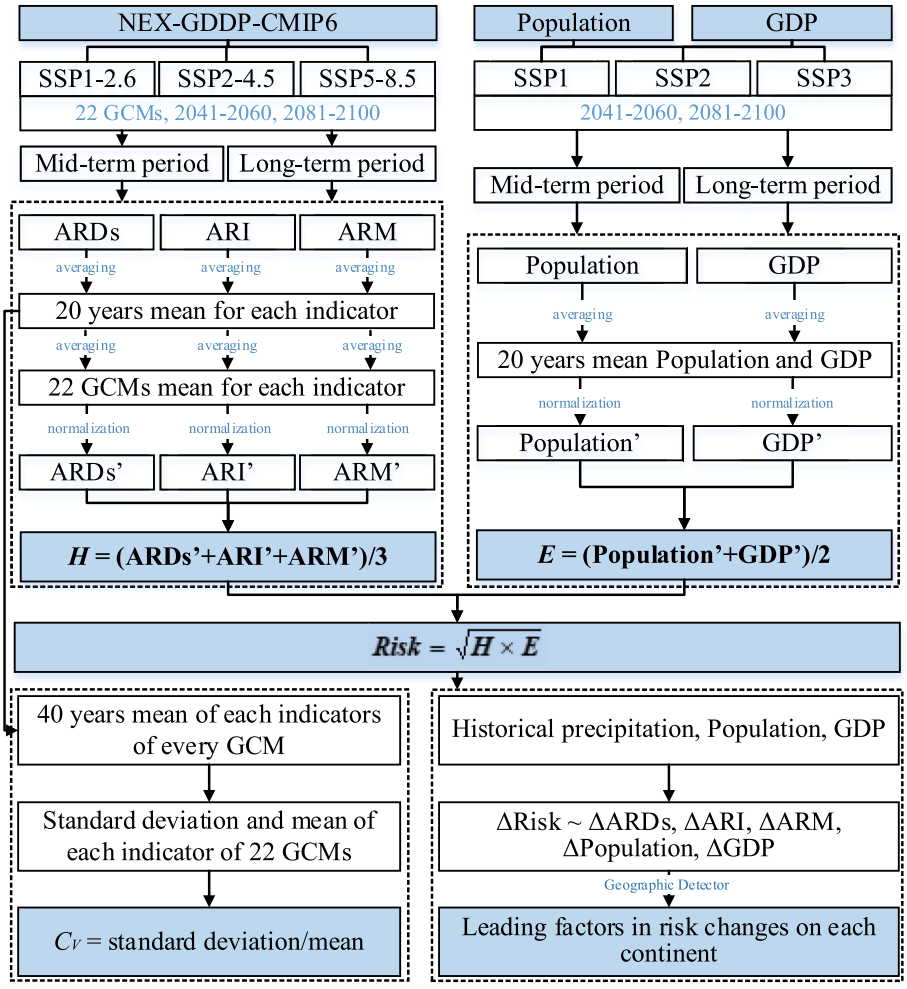

Fig. 1. Technology flowchart.

index of SSP1-2.6 corresponds to the exposure index of SSP1, the hazard index of SSP2-4.5 corresponds to the exposure index of SSP2, and the hazard index of SSP5-8.5 corresponds to the exposure index of SSP3. Finally, we used the natural breakpoint method (Anchang et al., 2016; Jenks and Caspall, 1971) to grade socioeconomic risks and obtained five risk grades.

2.2.4. Analysis of the uncertainty based on the coefficient of variation

The coefficient of variation is the ratio of the standard deviation and the average of the original data (Eq. (2)). It has no unit and can be used to compare the dispersions of quantitative variables that are not expressed in the same units, or the dispersions of variables that have very different mean. Therefore, we used the coefficient of variation to analyze the difference in rainstorm hazard calculated from different GCM simulation data grid by grid. The greater the coefficient of variation, the greater the uncertainty of the rainstorm risk assessment results.

$$c_v = \frac{\sigma}{\mu} \tag{2}$$

where σ is the standard deviation of a set original data; μ is the average of a set original data; and c_v represents the coefficient of variation.

2.2.5. Analysis of the leading factors causing spatial differences in risk changes on each continent based on the geographic detector

The geographic detector is a statistical tool to detect spatial heterogeneity and explore the determinants behind spatial heterogeneity (Wang et al., 2010, 2016). It is widely used in the study of driving factors such as the evolution of the spatial distribution patterns of ground objects (Guo et al., 2022; Wei et al., 2022; Zhu et al., 2022). We used the factor detector in the geographic detector to measure the interpretation degree between the socioeconomic risk changes of rainstorms and the changes of socioeconomic exposure and three rainstorm indicators. The calculation formula (Wang et al., 2016) of the q value is as follows:

$$q = 1 - \frac{\sum_{h=1}^{L} N_h \sigma_h^2}{N\sigma^2} = 1 - \frac{SSW}{SST} = 1 - \frac{1}{1 + \frac{SSB}{SSW}} \tag{3}$$

$$SSW = \sum_{h=1}^{L} N_h \sigma_h^2 \tag{4}$$

$$SST = N\sigma^2 = SSW + SSB \tag{5}$$

Let's assume that factor is X and the variable is Y, where q is the interpretation degree value of factor X to the spatial heterogeneity of variable Y; $h = 1, \ldots, L$ refers to the stratification of variable Y or factor X; N_h and N are the number of units of the strata and the whole study area, respectively; σ_h^2 is the variance of the values of the variable Y of the strata h; σ^2 is the population variance of values of the variable Y of the whole study area; SSW, SSB and SST are the sum of intra-strata variance, the sum of between-strata variance, and the total sum of variance, respectively.

The range of q values is [0,1]. A larger q-value indicates a stronger stratified heterogeneity effect of Y. This means that the stratification is able to explain a larger proportion of the total variation in the data.

When the q-value is small, it suggests that either SSW is large or SSB is small. In either case, the within-stratum variation is relatively large compared to the between-stratum variation, indicating weakly stratified heterogeneity. Therefore, a larger q-value indicates a stronger ability to explain the variation between strata, and thus a stronger stratified heterogeneity effect. If stratification is generated by variable X, the larger the q value, the stronger the explanatory power of the independent variable X for attribute Y, and vice versa.

3. Results

3.1. Hazard analysis of future rainstorms

Fig. 2 is the distribution map of the rainstorm hazard index under the three future scenarios, SSP1-2.6, SSP2-4.5, and SSP5-8.5, in the mid-term and long-term periods. The figure shows that the regions with the largest rainstorm hazard index are mainly distributed in the western and southeastern coastal areas of North America, the northwestern and southeastern regions of South America, the western and southeastern regions of Africa, the southern and southeastern regions of Asia, and the northern region of Oceania. The average global hazard indices of the SSP1-2.6, SSP2-4.5, and SSP5-8.5 scenarios in the mid-term period are 0.0313, 0.0321, and 0.0344, respectively. Compared to the mid-term period, the average global hazard indices for the three scenarios of SSP1-2.6, SSP2-4.5, and SSP5-8.5 in the long-term period have increased by 1.60 %, 12.15 %, and 36.63 %, respectively. From the perspective of continents (Fig. 3), the value and distribution of the rainstorm hazard index differ among the six continents, with the hazard index ranging from 0.0078 to 0.1019, among which Oceania has the largest average hazard index, followed by South America, and Europe has the smallest hazard index. South America has the largest standard deviation of the hazard index, followed by Oceania, and Europe has the smallest standard deviation of the hazard index. Compared with the mid-term period, the hazard indices of the six continents in the long-term period increase by 0.33 %-2.64 % on average under the SSP1-2.6 scenario, 10.02 %-13.13 % on average under the SSP2-4.5 scenario, and 22.46 %-58.07 % on average under the SSP5-8.5 scenario. In the three future scenarios, the average increasing rate of the rainstorm hazard index in Africa is the largest, followed by Asia, and the smallest increasing rate is projected to occur in Oceania.

3.2. Socioeconomic exposure to future rainstorms

Fig. 4 shows the curve of the global population and GDP under the historical and three future scenarios. Fig. 4 (a) shows that the global population in 1980–2010 basically showed a trend of constant growth. In the future, the global population in the SSP3 scenario is projected to be the largest, followed by the SSP2 scenario, and the global population in the SSP1 scenario is projected to be the smallest. Under the SSP1 scenario, the growth rate of the population will slow down during 2020–2050, and the total global population will decrease during 2050–2100. Under the SSP2 scenario, the growth rate of the global population is projected to gradually slow down during 2020–2070, and the total global population is projected to slowly decrease during 2070–2100. Under the SSP3 scenario, the global population is projected to increase at a constant rate. Fig. 4 (b) shows that the total global GDP has an increasing trend from 2020 to 2100 under the three scenarios. The total global GDP is projected to be the largest under the SSP1 scenario and the smallest under the SSP3 scenario. Under the SSP1 scenario, GDP first grows rapidly and then slowly. The growth rate of GDP under the SSP2 scenario is accelerating, and the total global GDP of the SSP2 scenario is expected to exceed that of the SSP1 scenario after 2100. Under the SSP3 scenario, the total global GDP is expected to increase slowly.

Fig. 5 shows the distribution of the socioeconomic exposure index under the three future scenarios, SSP1-2.6, SSP2-4.5, and SSP5-8.5, in

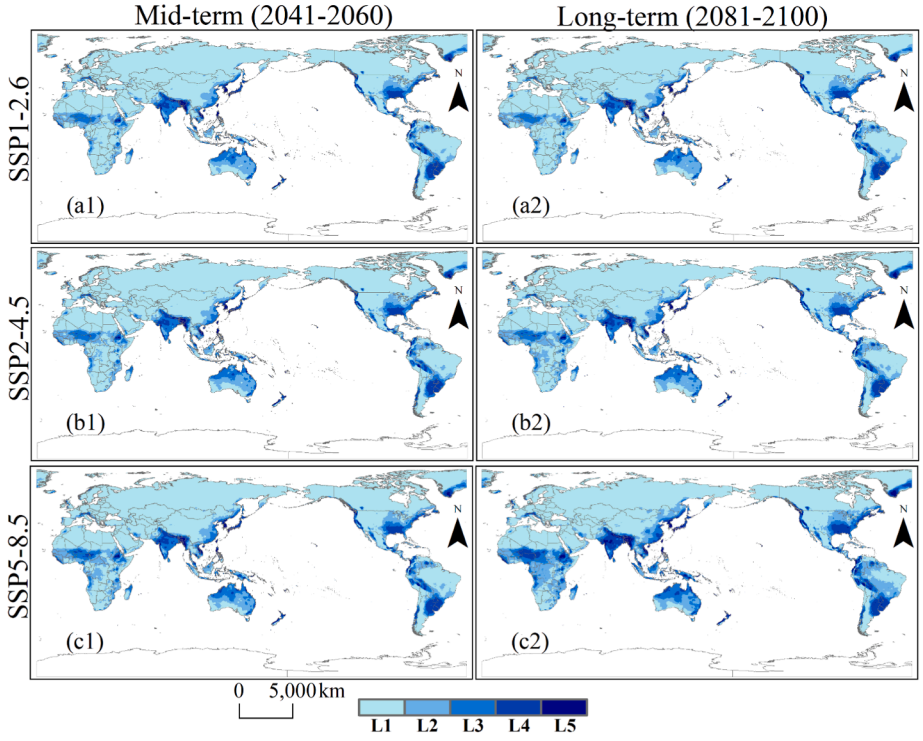

(L1: 0-0.027; L2: 0.027-0.088; L3: 0.088-0.176; L4: 0.176-0.307; L5: 0.307-0.775.)

Fig. 2. Distribution of the rainstorm hazard index under the three scenarios (SSP1-2.6, SSP2-4.5, and SSP5-8.5) in the two future periods, where (1) is the mid-term (2041–2060) and (2) is the long-term (2081–2100).

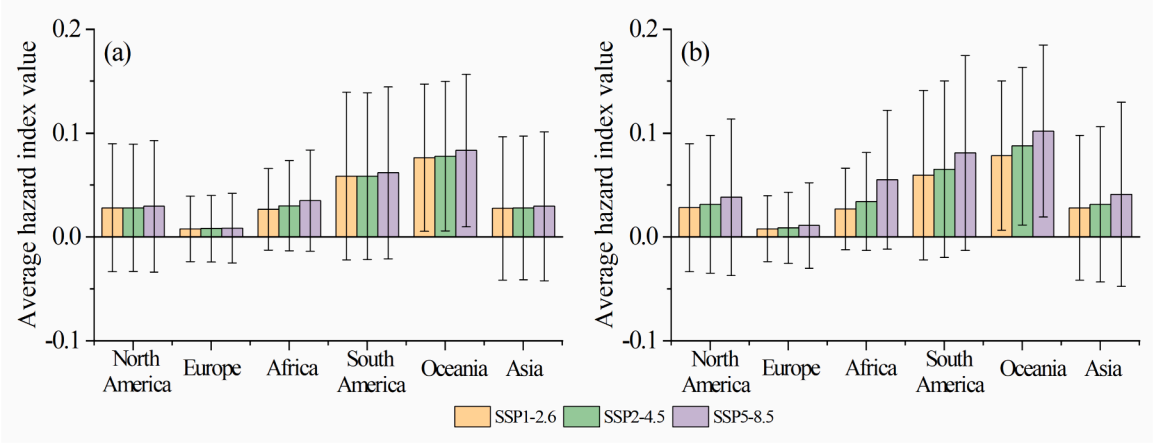

Fig. 3. Mean and standard deviation of the hazard index of the six continents in the(a) mid-term (2041–2060) and (b) long-term (2081–2100) of the 21st century.

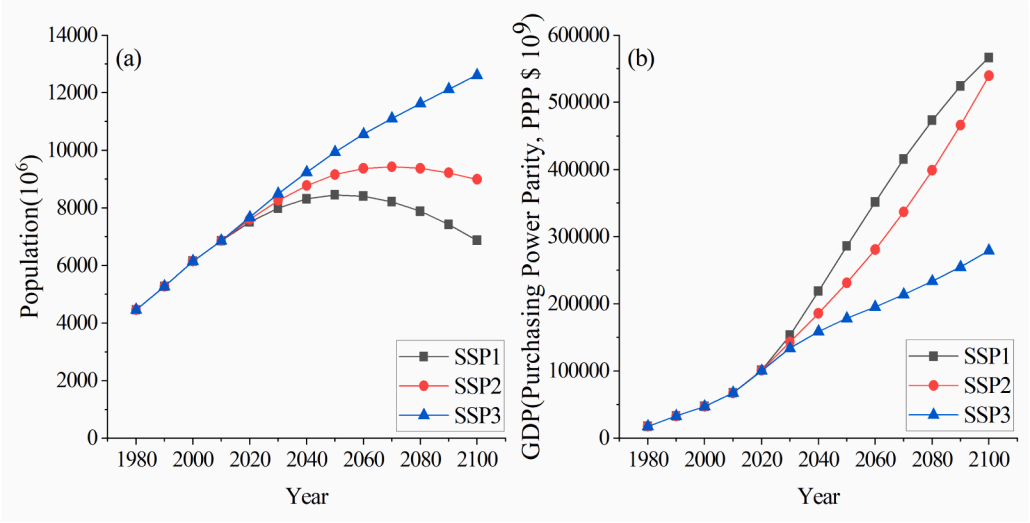

Fig. 4. Changes in global (a) population and (b) GDP under the historical (1980–2010) and future (2020–2100) scenarios.

the mid-term and long-term periods. Overall, there are more regions with higher exposure indices in China and India. In the mid-term period, the average value of the global socioeconomic exposure index is almost equal under the SSP1 and SSP2 scenarios, and both are greater than that under the SSP3 scenario. In the long-term, the average value of the global socioeconomic exposure index is the largest under the SSP2 scenario, followed by the SSP1 scenario, and is the smallest under the SSP3 scenario. The average global socioeconomic exposure index in the long-term period increases by 23.51 % under SSP1, 24.96 % under SSP2, and 19.63 % under SSP3 compared with the average global socioeconomic exposure index in the mid-term period. From the perspective of continents, both the average value and standard deviation of the socioeconomic exposure index are the smallest in Oceania. The average value of socioeconomic exposure in Oceania is 0.00011–0.00024 and the standard deviation is 0.0010–0.0026. Compared with the mid-term period, the average socioeconomic exposure index of the six continents in the long-term period increases by 0.62 %-69.56 % under the SSP1 scenario, 13.43 %-76.33 % under the SSP2 scenario, and −5.11 %-66.47 % under the SSP3 scenario. Among them, the socioeconomic exposure index increases the most under all three future scenarios in Africa and increases the least in Asia under the SSP1 and SSP2 scenarios and in Europe under the SSP3 scenario.

3.3. Socioeconomic risk analysis of future rainstorms

Fig. 6 shows the distribution of socioeconomic risk levels of rainstorms in the mid-term and long-term periods under the three future scenarios, SSP1-2.6, SSP2-4.5, and SSP5-8.5. The socioeconomic risk of rainstorms in most regions of the world is at the first level. The regions with the greatest socioeconomic risk are concentrated in southern and southeastern Asia, especially China and India. Under the SSP1-2.6, SSP2-4.5, and SSP5-8.5 scenarios, the average socioeconomic risk of global rainstorms in the long-term period increases by 4.04 %, 16.66 % and 27.30 %, respectively, compared with that in the mid-term period. From the perspective of the continents (Fig. 7), under the three future scenarios in the two future periods, Asia has the largest socioeconomic risks, while Europe has the smallest socioeconomic risks. In general, compared with the mid-term period, the number of grids with high-risk levels (Levels 4 and 5) on each continent increases at the end of the 21st century.

4. Discussion

4.1. Uncertainty of rainstorm indicators

To reduce the uncertainty of model simulation, we used precipitation datasets simulated by 22 GCMs in CMIP6 as input to analyze the

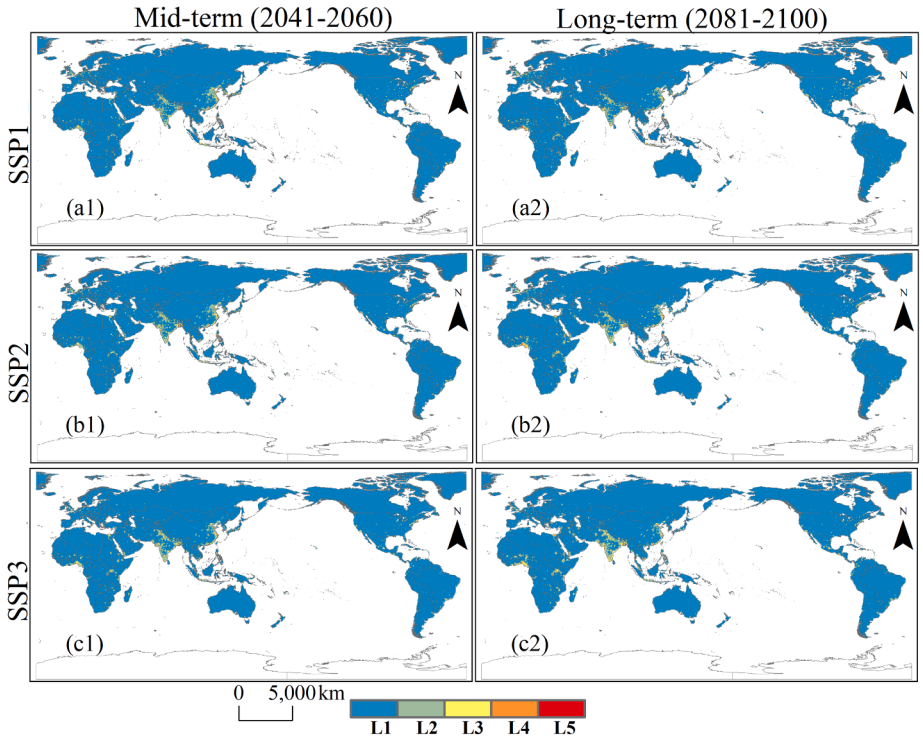

(L1: 0-0.006; L2: 0.006-0.025; L3: 0.025-0.070; L4: 0.070-0.177; L5: 0.177-0.355.)

Fig. 5. Distribution of the socioeconomic exposure index under the three scenarios (SSP1, SSP2, and SSP3) in the two future periods, where (1) is the mid-term (2041–2060) and (2) is the long-term (2081–2100)).

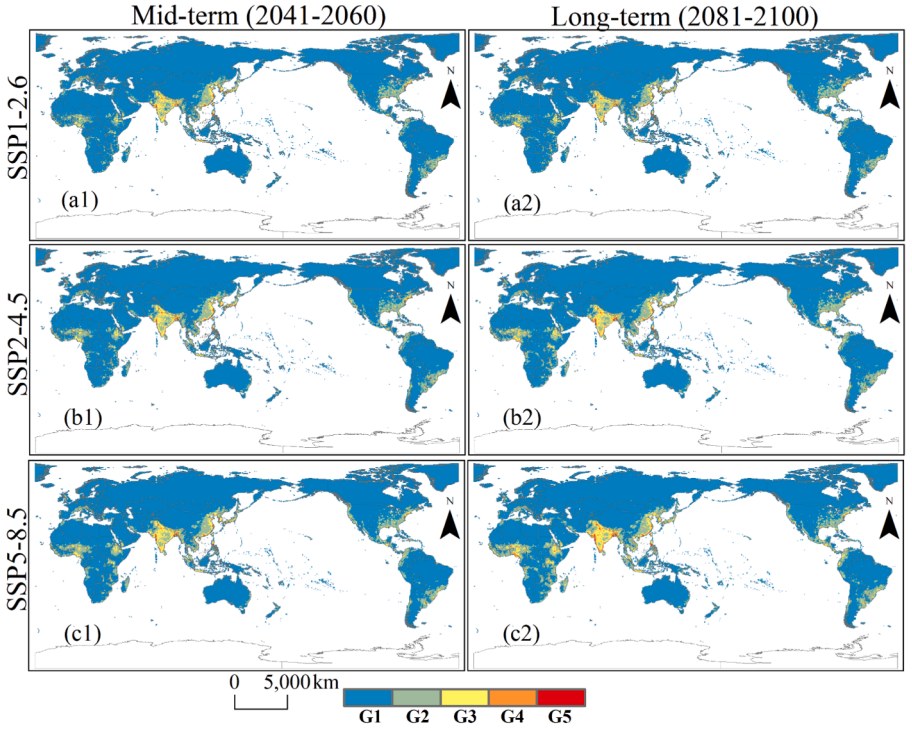

(G1: 0-0.006; G2: 0.006-0.024; G3: 0.024-0.061; G4: 0.061-0.151; G5: 0.151-0.475.)

Fig. 6. Distribution of socioeconomic risk under the three scenarios (SSP1-2.6, SSP2-4.5, and SSP5-8.5) in the two future periods, where (1) is the mid-term (2041–2060) and (2) is the long-term (2081–2100).

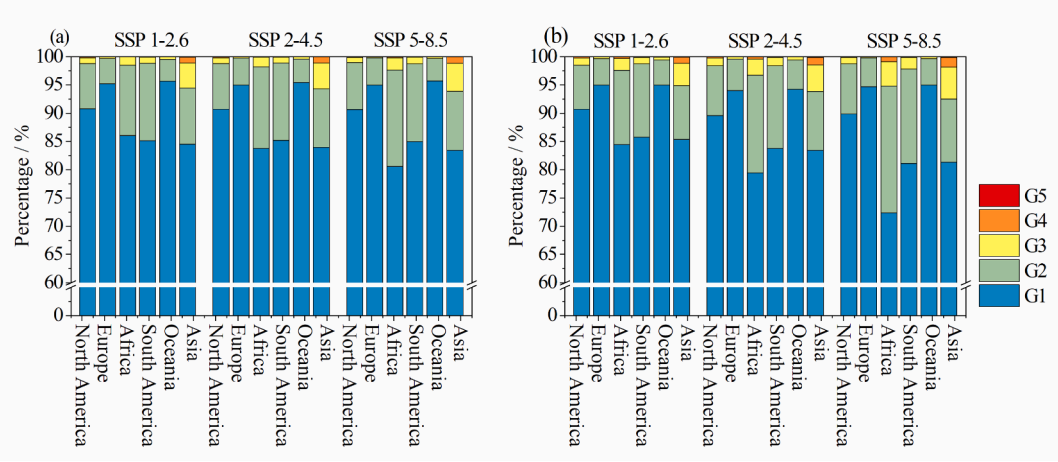

(G1: 0-0.006; G2: 0.006-0.024; G3: 0.024-0.061; G4: 0.061-0.151; G5: 0.151-0.475.)

Fig. 7. Distribution of five socioeconomic risk levels on six continents in the two future periods, where (a) is mid-term (2041–2060) and (b) is long-term (2081–2100).

rainstorm hazard. The final ARDs, ARI, and ARM were all calculated according to the mean value of the 22 GCMs. In this study, we calculated the coefficient of variation of ARDs/ARI/ARM from the 22 GCMs for the historical period (Fig. 8) and two future time periods (2041–2060 and 2081–2100) under three scenarios (the SSP1-2.6, SSP2-4.5, and SSP5-8.5) (Fig. 9 and Fig. 10) to measure the uncertainty of ARDs/ARI/ARM. Overall, the distribution of the coefficient of variation calculated for the three indicators, three periods, and three scenarios is similar and the regions with the greatest uncertainty are concentrated in central North America, Central America, central and southern Africa, central South America, eastern Asia, and southern Oceania. During the historical period, the global average values of the coefficients of variation of ARDs, ARI, and ARM are 0.7279, 0.7095, and 0.7115. During the time period of 2041–2060, the global average values of the coefficients of variation of ARDs, ARI, and ARM are 0.7750, 0.7459, and 0.7493 under the SSP1-2.6 scenario, 0.8197, 0.7822, and 0.7866 under the SSP2-4.5 scenario, and are 0.8297, 0.7864, and 0.7914 under the SSP5-8.5 scenario, respectively. During the time period of 2081–2100, the global average values of the coefficients of variation of ARDs, ARI, and ARM are 0.7882, 0.7579, and 0.7615 under the SSP1-2.6 scenario, 0.8128, 0.7693, and 0.7746 under the SSP2-4.5 scenario, and are 0.8584, 0.7654, and 0.7754 under the SSP5-8.5 scenario, respectively. Thus, among the three scenarios, the SSP5-8.5 scenario has the largest uncertainty; and among the three rainstorm indicators, ARDs have the largest uncertainty. Some studies that have only used the rainstorm frequency (such as ARDs) (Shi et al., 2021; Sun et al., 2021; Tang and Hu, 2022) to calculate the rainstorm risk may suffer from high uncertainty. This study comprehensively uses three rainstorm indicators, ARDs, ARI, and ARM, which can reduce the uncertainty of rainstorm hazard assessment caused by the uncertainty of a single rainstorm indicator to a certain extent.

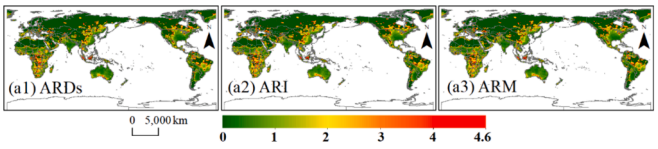

Fig. 8. Distribution of coefficients of variation of ARDs, ARI, and ARM among 22 models under the historical scenario.

4.2. Socioeconomic risk changes

To analyze the change in future rainstorm risk relative to the historical period, we first used the historical precipitation data of 22 GCMs to calculate the rainstorm hazard index in terms of the method introduced in Section 2.2.1. Then, we calculated the socioeconomic exposure index based on the population and GDP from 1991 to 2010 obtained from the NIES, Japan, in terms of the method introduced in Section 2.2.2. Finally, we calculated the historical socioeconomic risk according to the method introduced in Section 2.2.3 and subtracted the historical socioeconomic risk from the socioeconomic risk under the future climate scenarios to obtain the changing value of socioeconomic risk. The results are shown in Fig. 11.

Fig. 11 shows that the socioeconomic risk of rainstorms in most regions of the world is projected to have an increasing trend, with the largest increase under the SSP5-8.5 scenario. Specifically, under the SSP5-8.5 scenario, the number of grids with increased risk in the mid-term and long-term is 97.58 % and 97.98 %, respectively. Under the SSP1-2.6 scenario, the number of grids with increased risk in the mid-term and long-term is 89.20 % and 86.57 %, respectively. The regions with the largest increase in the socioeconomic risk of rainstorms are mainly distributed on the southwestern coasts of Africa and the southern and southeastern coasts of Asia, which are also the regions with large rainstorm hazards (Fig. 2) and high socioeconomic exposures (Fig. 5). In general, compared with the historical period, the socioeconomic risks of rainstorms on the eastern coast of China, the central and southern parts of India, Nigeria, and its surrounding areas, southern Mexico, the western coast of Colombia, and the southeastern coast of Brazil increase significantly. Compared to other regions where rainstorm hazards will also increase significantly, these areas are expected to experience the most substantial growth in population and GDP in future scenarios, thus eventually leading to the most prominent increase in rainstorm risk.

Fig. 12 shows the correlation between the changes in rainstorm socioeconomic risk and the changes in three rainstorm indices (ARDs, ARI, and ARM) and socioeconomic exposure (population and GDP) in the mid-term and long-term periods under the three future scenarios, SSP1-2.6, SSP2-4.5, and SSP5-8.5. In the figure, the larger the q value is, the stronger the interpretation ability. Under the SSP1-2.6 scenario, the socioeconomic risk changes of rainstorms in Europe are most closely related to the three rainstorm indices, with q values between socioeconomic risk changes and rainstorm indices ranging from 0.4075 to 0.4141 in the mid-term period and 0.3203–0.3340 in the long-term period. The

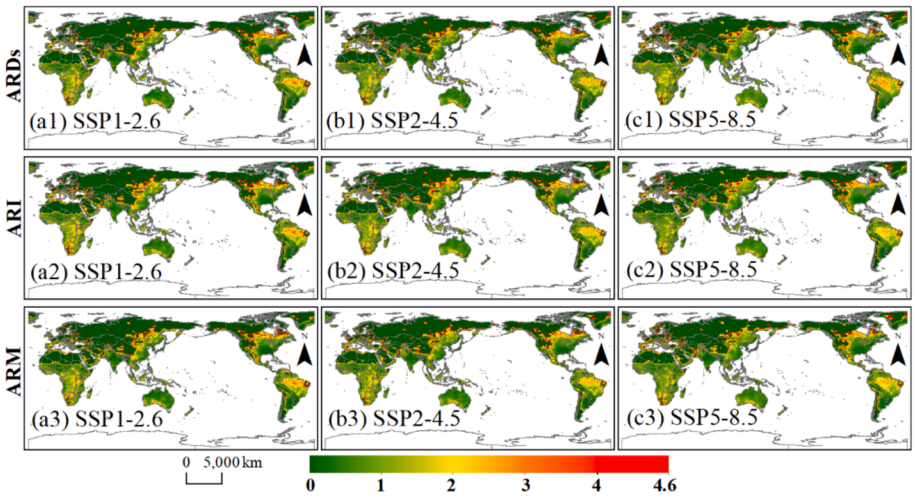

Fig. 9. Distribution of coefficients of variation of ARDs, ARI, and ARM among 22 models under the SSP1-2.6, SSP2-4.5, and SSP5-8.5 scenarios of 2041–2060.

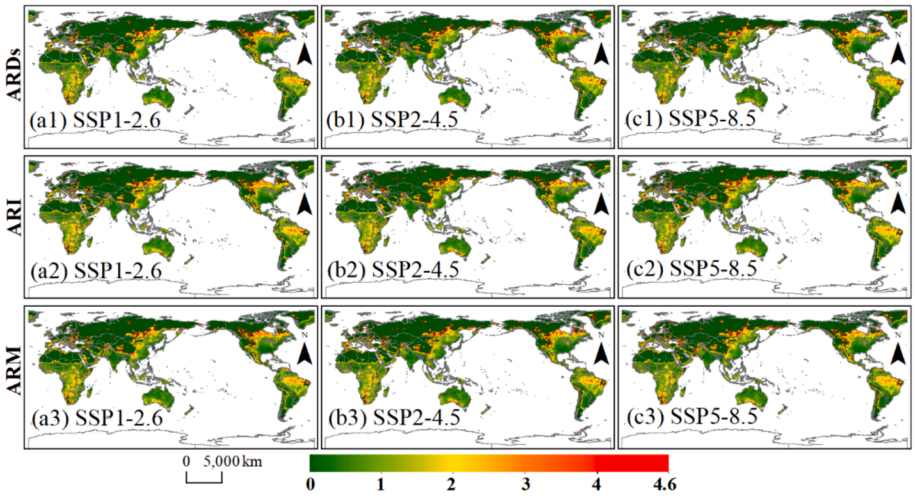

Fig. 10. Distribution of coefficients of variation of ARDs, ARI, and ARM among 22 models under the SSP1-2.6, SSP2-4.5, and SSP5-8.5 scenarios of 2081–2100.

q value between rainstorm socioeconomic risk changes and socioeconomic exposure on five continents except Europe is between 0.49 and 0.88, which is greater than the q value between socioeconomic risk changes and the three rainstorm indices. The socioeconomic risk changes of rainstorms in Africa are most closely related to population changes, while the socioeconomic risk changes of rainstorms in North and South America and Asia are most closely related to GDP changes. The socioeconomic risk changes of rainstorms in Oceania are least closely related to rainstorm indices. Similar conclusions can be made under the SSP2-4.5 and SSP5-8.5 scenarios. The results are consistent with the existing research results (Chen and Sun, 2021; Liu et al., 2020b).

For areas where the risk of rainstorms increases due to the increase in rainstorm hazard, such as Europe, the construction of a meteorological monitoring system should be strengthened and the disaster warning system should be improved (Alfieri et al., 2012; Calvello et al., 2020). For example, advanced meteorological prediction models and big data analysis should be used to improve the accuracy of rainstorm event prediction (Shabariram et al., 2016), and early warning of possible rainstorm events should be given in advance to ensure that accurate disaster information is transmitted to the public (Hallegatte, 2012; Pappenberger et al., 2015). In case of a rainstorm, emergency response can be carried out timely and effective. For areas with increased rainstorm risk caused by increased exposure of rainstorm-bearing bodies, such as North and South America, Africa, Asia, and Oceania, the layout of the city should be reasonably planned to avoid vigorously developing areas that are susceptible to flooding, improve the efficiency of urban drainage systems, and strengthen flood prevention facilities (Fraiture et al., 2017), such as building flood control dams and widening drainage channels. In addition, protecting natural wetlands and water sources to alleviate the rapid concentration of rainwater in cities (Kim et al., 2016; Douglas, 2018). Promoting afforestation, increasing vegetation coverage, reducing soil erosion, and improving soil flood resistance are also beneficial for reducing flood risks (Liu et al., 2020a; Takata and Hanasaki, 2020).

4.3. Contributions and limitations

Compared with previous studies, this study has the two following characteristics:

First, there is still great uncertainty about future climate change (Alves et al., 2021; Dey et al., 2019; Long and Li, 2021; Ortega et al., 2021; Zappa and Shepherd, 2017). The simulation performance of GCMs is related to various factors such as model structure and parameter settings, initialization conditions, etc. Numerous studies have shown that no GCM performs well in different scenarios, such as different regions, terrain conditions, climate zones, seasons, etc. There is also no research confirming that a certain GCM performs better than other

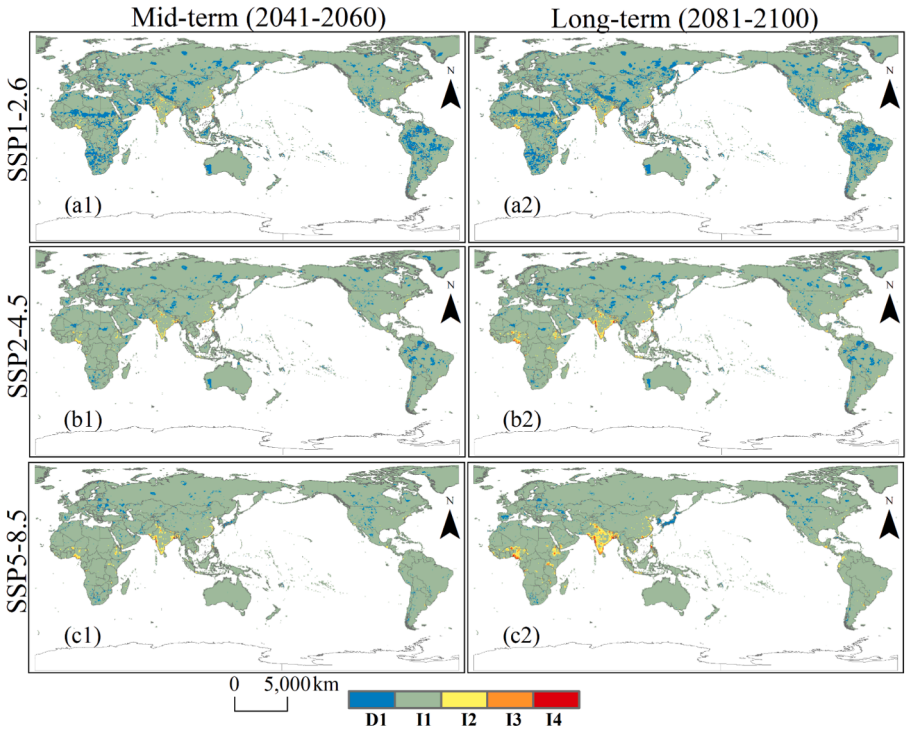

Fig. 11. Socioeconomic risk change distribution under three scenarios (SSP1-2.6, SSP2-4.5, and SSP5-8.5) in the two future periods, where (1) is the mid-term (2041–2060) and (2) is the long-term (2081–2100). (Note: D represents a decrease, I represents an increase, and D1 < I1 < I2 < I3 < I4).

GCMs. Using only one GCM simulation data for analysis has significant uncertainty. Compared to a single model, the multi-model ensemble average demonstrates superior simulation capabilities and can effectively reduce model uncertainty. Methods of the multi-model ensemble include the arithmetic mean (Santer et al., 2007; Duan and Phillips, 2010; Sillmann et al., 2013; Miao et al., 2014; Fu et al., 2018; Sonkoué et al., 2019; Sun et al., 2021; Shi et al., 2021), the weighted mean (Duan and Phillips, 2010; Niu et al., 2018; Xu et al., 2023), and the median (Sillmann et al., 2013; Srivastava et al., 2020). The mean method is the most commonly used method among the three methods. Therefore, this study also chose to use an arithmetic mean as a method of the multi-model ensemble. Specifically, we used the future daily precipitation data of 22 GCMs in CMIP6 to calculate three rainstorm indices (ARDs, ARI, and ARM).

Second, the hazard of a rainstorm disaster is related to many characteristics of rainstorms, such as frequency, intensity, and duration (Wu et al., 2010; Feng et al., 2019; Deng et al., 2022). Comprehensive consideration of multiple rainstorm characteristics can more comprehensively evaluate the hazard of rainstorms and avoid the deviation and limitation caused by a single factor (Bécue-Bertaut and Pagès, 2008; Chen et al., 2020; Liu et al., 2022). In addition, many previous studies have considered the population and the economy separately and calculated population exposure and economic exposure in disasters (Lim et al., 2018; Mondal et al., 2021; Chen and Sun, 2021; Chen et al., 2021; Zhao et al., 2022; Xie et al., 2022), which is not conducive to the comprehensive analysis of socioeconomic risks. Therefore, using the arithmetic mean method, ARDs, ARI, and ARM were integrated into a hazard index, while population and GDP were integrated into an exposure index in this study. The weighted average method requires sophisticated mathematical models (such as the Analytic Hierarchy Process, Fuzzy Analytic Hierarchy Process, Entropy Weight Method, and Principal Component Analysis) to capture the complex relationships and mutual influences between elements, thereby determining the importance and priority of different elements. On the one hand, weights are influenced by model performance and subjective factors. On the other hand, the importance of various elements in different regions of the world is theoretically different, and weights need to be set by region, but this is difficult to achieve. Different from weighted average, the advantage of arithmetic mean is that the calculation process is simple, does not require too many assumptions and prerequisites, and can provide a relatively stable comprehensive indicator. Based on the risk assessment paradigm of UNDRR, the risk index can be expressed as the product of the hazard index and exposure index (United Nations Office for Disaster Risk Reduction, 2019). After obtaining the exposure index and hazard index, we further integrated them into a risk index through geometric averaging. Compared to the arithmetic mean, the geometric mean is more suitable for indicators that handle product relationships, especially indicators such as ratios and proportions. The geometric mean of two indices and the product of two indices have the same trend, but with larger values, making it easier to observe differences.

However, there are also some limitations in this paper. First, global-scale rainstorm socioeconomic risk analysis was conducted based on NEX-GDDP-CMIP6 future precipitation simulation data. However, the NEX-GDDP-CMIP6 data resolution is relatively coarse, which is not conducive to analysis in local areas. In the future, it is necessary to combine regional climate models to produce a regional climate simulation dataset with higher resolution by downscaling to better support the accurate analysis of small-scale rainstorm disasters. Second, there are many different choices for rainstorm thresholds. Considering the global comparability, this paper chose 50 mm daily precipitation as the threshold to identify a rainstorm. However, for local areas, we can use the threshold selection method suitable for the local area to conduct fine-resolution research in combination with higher-resolution datasets to better serve the formulation of disaster prevention and mitigation policies in local areas. Third, this paper used the population and GDP simulation data in the future scenario as the disaster-bearing body. For the population, different conditions, such as age, educational background, and health status, will have large differences in disaster-bearing

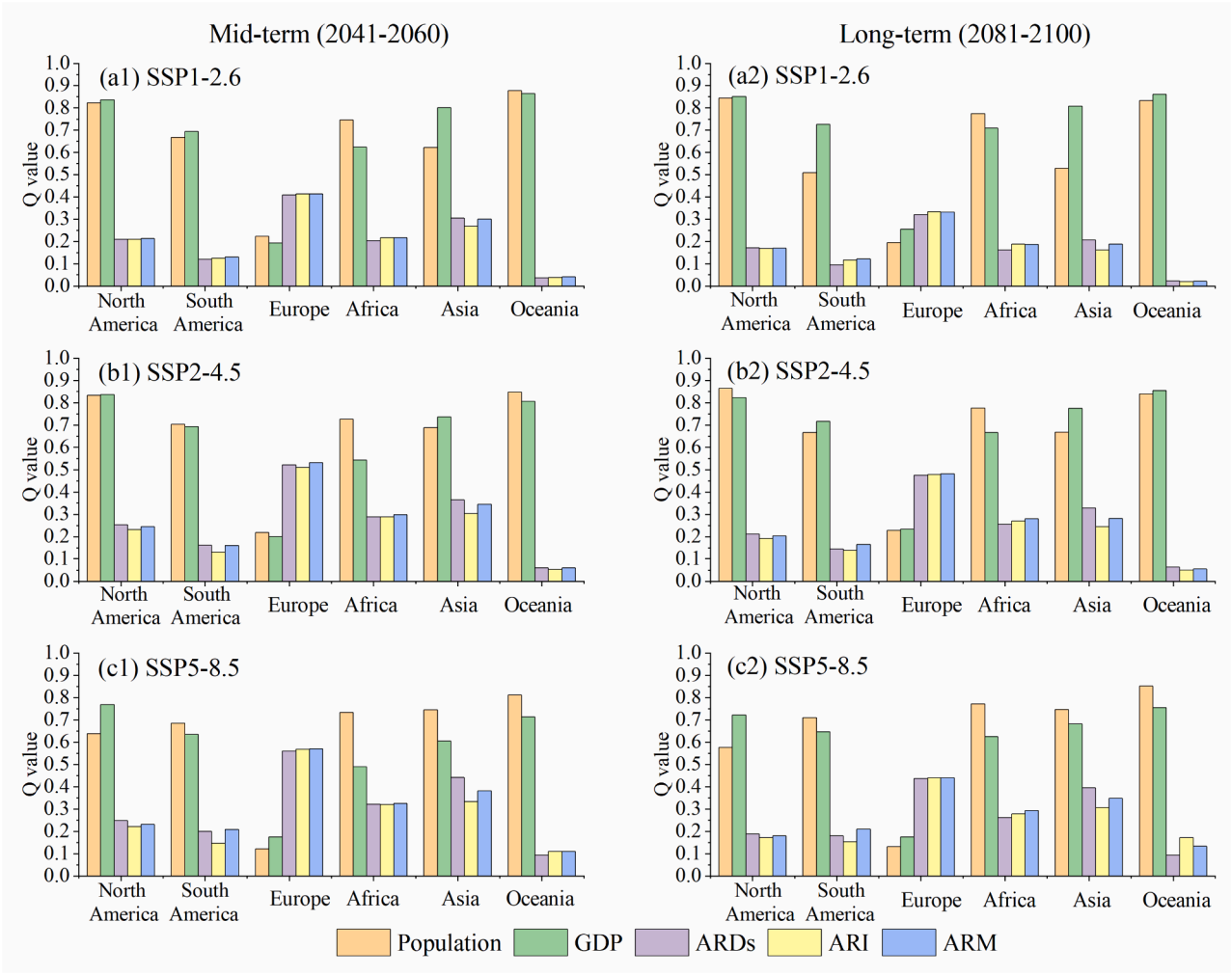

Fig. 12. Interpretation degree of population, GDP, ARDs, ARI, and ARM to the spatial heterogeneity of socioeconomic risk changes in 6 continents under three scenarios (SSP1-2.6, SSP2-4.5, SSP5-8.5) in the two future periods, where (1) is the mid-term (2041–2060) and (2) is the long-term (2081–2100).

capacity, but more refined population data will also have greater uncertainty. Based on our study, rainstorm risk changes in most regions are more closely related to changes in population and GDP. The accuracy and uncertainty of disaster-bearing body data will greatly affect the results of risk assessment. Therefore, our study highlights that while producing more refined and precise precipitation datasets, it is also necessary to strengthen the production and research of disaster-bearing body data such as population and GDP. Fourth, the disaster-bearing body of rainstorms not only includes population and GDP, but also includes social infrastructure and urban buildings (Bonazza et al., 2021; Yang et al., 2024) and so on. However, due to limitations in the availability of these data in future scenarios, this study like most previous studies did not consider other disaster-bearing bodies of rainstorms other than population and GPD, which may affect the results to some extent. In the future, with the gradual enrichment of prediction data of disaster-bearing bodies, we can add them to the assessment of rainstorm risk in order to improve the accuracy of the assessment results. In addition, we may be able to use the latest data of disaster-bearing bodies such as infrastructure and buildings to conduct a rainstorm risk assessment in combination with future rainstorm hazard data. Although the infrastructure and buildings in the future cannot remain unchanged, the rainstorm risk assessment results considering the infrastructure and buildings and other disaster-bearing bodies are theoretically more accurate.

5. Conclusions

This paper uses the precipitation simulation data of 22 GCMs of CMIP6 and the population and GDP data of different scenarios in the future to calculate the socioeconomic risks of rainstorms in the mid-term and long-term periods under three scenarios (SSP1-2.6, SSP2-4.5, and SSP5-8.5) and further explores the uncertainty between the data of the 22 GCMs used in this study and the changes in the socioeconomic risks of rainstorm relative to historical periods and their leading factors. The main conclusions are as follows:

First, from a global perspective, compared with the mid-term period, under the three scenarios (SSP1-2.6, SSP2-4.5, and SSP5-8.5), the mean hazard index of rainstorms increases by 1.60 %, 12.15 %, and 36.63 %, respectively, and the mean socioeconomic exposure index increases by 23.51 %, 24.96 %, and 19.63 % in the long-term period, respectively. From the perspective of continents, the mean value of the rainstorm hazard index under the three future scenarios is the largest in Oceania, followed by South America, and is the smallest in Europe. Compared with the mid-term period, the hazard index of rainstorms in the long-term period increases the most in Africa, followed by Asia, and is the least in Oceania. The average socioeconomic exposure index is the largest in Asia, followed by Africa, and is the smallest in Oceania. However, compared with the mid-term period, the largest increase in socioeconomic exposure is in Africa all the time under the three scenarios in the long-term period, but the continents with the smallest

increase differ under the three scenarios.

Second, from a global perspective, the socioeconomic risk of rainstorms in most regions of the world will increase in the future, with the largest increase in the SSP5-8.5 scenario and the smallest increase in the SSP1-2.6 scenario. Under the lowest growth scenario (SSP1-2.6 scenario in the long-term period), the proportion of the grid with increased socioeconomic risk of rainstorms is also above 86.57 %. The average socioeconomic risk of rainstorms in the long-term period increases by 4.04 % under SSP1-2.6, 16.66 % under SSP2-4.5, and 27.30 % under SSP5-8.5 compared with that in the mid-term period. In general, the socioeconomic risks of rainstorms on the eastern coast of China, the central and southern parts of India, Nigeria and its surrounding areas, southern Mexico, the western coast of Colombia, and the southeastern coast of Brazil are projected to increase significantly.

Finally, the change in rainstorm socioeconomic risk in North and South America, Africa, Asia, and Oceania is more related to socioeconomic exposure, and the change in rainstorm socioeconomic risk in Europe is more related to the three rainstorm indicators.

CRediT authorship contribution statement

Xiufang Zhu: Funding acquisition, Formal analysis, Data curation, Conceptualization. **Mingxiu Tang:** Writing – review & editing, Writing – original draft, Formal analysis, Data curation, Conceptualization. **Tingting Liu:** Writing – review & editing. **Chunhua Guo:** Writing – review & editing.

Declaration of competing interest

The authors declare that they have no known competing financial interests or personal relationships that could have appeared to influence the work reported in this paper.

Data availability

The data that has been used is confidential.

Acknowledgments

This work was supported by the National Natural Science Foundation of China (Grant No. 42077436). We thank the anonymous reviewers for their valuable comments.

References

Abdila, W.P., Nugroho, B.D.A., 2021. Trend analysis of extreme precipitation indices in the southern part of Java. IOP Conf. Ser.: Earth Environ. Sci. 653, 012032 https://doi.org/10.1088/1755-1315/653/1/012032.

AghaKouchak, A., Chiang, F., Huning, L.S., Love, C.A., Mallakpour, I., Mazdiyasni, O., Moftakhari, H., Papalexiou, S.M., Ragno, E., Sadegh, M., 2020. Climate Extremes and Compound Hazards in a Warming World. Annual Review of Earth and Planetary Sciences 48, 519–548. https://doi.org/10.1146/annurev-earth-071719-055228.

Alfieri, L., Salamon, P., Pappenberger, F., Wetterhall, F., Thielen, J., 2012. Operational early warning systems for water-related hazards in Europe. Environ. Sci. Policy 21, 35–49. https://doi.org/10.1016/j.envsci.2012.01.008.

Alves, L.M., Chadwick, R., Moise, A., Brown, J., Marengo, J.A., 2021. Assessment of rainfall variability and future change in Brazil across multiple timescales. Int J Climatol 41. https://doi.org/10.1002/joc.6818.

Anchang, J.Y., Ananga, E.O., Pu, R., 2016. An efficient unsupervised index based approach for mapping urban vegetation from IKONOS imagery. International Journal of Applied Earth Observation and Geoinformation 50, 211–220. https://doi.org/10.1016/j.jag.2016.04.001.

Ayugi, B., Jiang, Z., Iyakaremye, V., Ngoma, H., Babaousmail, H., Onyutha, C., Dike, V. N., Mumo, R., Ongoma, V., 2022. East African population exposure to precipitation extremes under 1.5 °C and 2.0 °C warming levels based on CMIP6 models. Environ. Res. Lett. 17, 044051 https://doi.org/10.1088/1748-9326/ac5d9d.

Bécue-Bertaut, M., Pagès, J., 2008. Multiple factor analysis and clustering of a mixture of quantitative, categorical and frequency data. Comput. Statist. Data Anal. 52, 3255–3268. https://doi.org/10.1016/j.csda.2007.09.023.

Bonazza, A., Sardella, A., Kaiser, A., Cacciotti, R., De Nuntiis, P., Hanus, C., Maxwell, I., Drdácký, T., Drdácký, M., 2021. Safeguarding cultural heritage from climate change related hydrometeorological hazards in Central Europe. Int. J. Disaster Risk Reduct. 63, 102455 https://doi.org/10.1016/j.ijdrr.2021.102455.

Bowles, D.C., Butler, C.D., Friel, S., 2014. Climate change and health in Earth's future. Earth's Future 2, 60–67. https://doi.org/10.1002/2013EF000177.

Calvello, M., Devoli, G., Freeborough, K., Gariano, S.L., Guzzetti, F., Kirschbaum, D., Nakaya, H., Robbins, J., Stähli, M., 2020. LandAware: a new international network on Landslide Early Warning Systems. Landslides 17, 2699–2702. https://doi.org/10.1007/s10346-020-01548-7.

Chen, J., Chen, M., Zhou, P., 2020. Using Multiple Index Comprehensive Method to Assess Urban Rainstorm Disaster Risk in Jiangsu Province. China. Mathematical Problems in Engineering 2020, e8973025.

Chen, H., Sun, J., 2020. Increased population exposure to precipitation extremes in China under global warming scenarios. Atmospheric and Oceanic Science Letters 13, 63–70. https://doi.org/10.1080/16742834.2020.1697168.

Chen, H., Sun, J., 2021. Significant Increase of the Global Population Exposure to Increased Precipitation Extremes in the Future. Earth's. Future 9. https://doi.org/10.1029/2020EF001941.

Chen, L., Wang, G., Miao, L., Gnyawali, K.R., Li, S., Amankwah, S.O.Y., Huang, J., Lu, J., Zhan, M., 2021. Future drought in CMIP6 projections and the socioeconomic impacts in China. International Journal of Climatology 41, 4151–4170. https://doi.org/10.1002/joc.7064.

Deng, M., Li, Z., Tao, F., 2022. Rainstorm Disaster Risk Assessment and Influence Factors Analysis in the Yangtze River Delta, China. Int. J. Environ. Res. Public. Health 19, 9497. https://doi.org/10.3390/ijerph19159497.

Dey, R., Lewis, S.C., Abram, N.J., 2019. Investigating observed northwest Australian rainfall trends in Coupled Model Intercomparison Project phase 5 detection and attribution experiments. International Journal of Climatology 39, 112–127. https://doi.org/10.1002/joc.5788.

Douglas, I., 2018. The challenge of urban poverty for the use of green infrastructure on floodplains and wetlands to reduce flood impacts in intertropical Africa. Landscape Urban Plan. 180, 262–272. https://doi.org/10.1016/j.landurbplan.2016.09.025.

Du, S., Wu, R., Sun, H., Yan, D., Xue, J., Liao, W., Tuo, Y., Zhang, W., 2022. Projection of Precipitation Extremes and Flood Risk in the China-Pakistan Economic Corridor. Frontiers in Environmental Science 10.

Duan, Q., Phillips, T.J., 2010. Bayesian estimation of local signal and noise in multimodel simulations of climate change. Journal of Geophysical Research: Atmospheres 115. https://doi.org/10.1029/2009JD013654.

Feng, Y., Li, Y., Zhang, Z., Gong, S., Liu, M., Peng, F., 2019. Multi-factor joint return period of rainstorms and its agricultural risk analysis in Liaoning Province, China. Geomatics, Natural Hazards and Risk 10, 1988–2008. https://doi.org/10.1080/19475705.2019.1660727.

Fraiture, C., Susanto, R., Suryadi, F.X., Wahyu, H.M., 2017. Urban Drainage Management and Flood Control Improvement Using the Duflow Case Study: Aur Sub Catchment, Palembang, South Sumatra. Indonesia. Makara Journal of Technology 21. https://doi.org/10.7454/mst.v21i2.3085.

Franzke, C.L.E., 2021. Towards the development of economic damage functions for weather and climate extremes. Ecological Economics 189, 107172. https://doi.org/10.1016/j.ecolecon.2021.107172.

Fu, Y.-H., Lu, R.-Y., Guo, D., 2018. Changes in Surface Air Temperature over China under the 1.5 and 2.0 °c Global Warming Targets. Adv. Clim. Change Res., including Special Topic on Mitigation for 1.5 ℃: Scenarios and Options 9, 112–119. https://doi.org/10.1016/j.accre.2017.12.001.

Guo, R., Zhu, X., Zhang, C., Cheng, C., 2022. Analysis of Change in Maize Plantation Distribution and Its Driving Factors in Heilongjiang Province. China. Remote Sensing 14, 3590. https://doi.org/10.3390/rs14153590.

Hallegatte, S., 2012. A Cost Effective Solution to Reduce Disaster Losses in Developing Countries: Hydro-Meteorological Services, Early Warning, and Evacuation. Policy Research Working Papers. the World Bank. https://doi.org/10.1596/1813-9450-6058.

Hauer, M.E., Hardy, D., Kulp, S.A., Mueller, V., Wrathall, D.J., Clark, P.U., 2021. Assessing population exposure to coastal flooding due to sea level rise. Nat Commun 12, 6900. https://doi.org/10.1038/s41467-021-27260-1.

Hu, X., Wang, M., Liu, K., Gong, D., Kantz, H., 2021. Using Climate Factors to Estimate Flood Economic Loss Risk. Int J Disaster Risk Sci 12, 731–744. https://doi.org/10.1007/s13753-021-00371-5.

Jenks, G.F., Caspall, F.C., 1971. Error on Choroplethic Maps: Definition, Measurement, Reduction. Annals of the Association of American Geographers 61, 217–244. https://doi.org/10.1111/j.1467-8306.1971.tb00779.x.

Kim, H., Lee, D.-K., Sung, S., 2016. Effect of Urban Green Spaces and Flooded Area Type on Flooding Probability. Sustainability 8, 134. https://doi.org/10.3390/su8020134.

Li, L., Zou, Y., Li, Y., Lin, H., Liu, D.L., Wang, B., Yao, N., Song, S., 2020. Trends, change points and spatial variability in extreme precipitation events from 1961 to 2017 in China. Hydrology Research 51, 484–504. https://doi.org/10.2166/nh.2020.095.

Lim, W.H., Yamazaki, D., Koirala, S., Hirabayashi, Y., Kanae, S., Dadson, S.J., Hall, J.W., Sun, F., 2018. Long-Term Changes in Global Socioeconomic Benefits of Flood Defenses and Residual Risk Based on CMIP5 Climate Models. Earth's Future 6, 938–954. https://doi.org/10.1002/2017EF000671.

Liu, Y., Chen, J., Pan, T., Liu, Y., Zhang, Y., Ge, Q., Ciais, P., Penuelas, J., 2020b. Global Socioeconomic Risk of Precipitation Extremes Under Climate Change. Earth's. Future 8. https://doi.org/10.1029/2019EF001331.

Liu, Y., Chen, J., 2021. Future global socioeconomic risk to droughts based on estimates of hazard, exposure, and vulnerability in a changing climate. Science of the Total Environment 751, 142159. https://doi.org/10.1016/j.scitotenv.2020.142159.

Liu, J., Hertel, T.W., Diffenbaugh, N.S., Delgado, M.S., Ashfaq, M., 2015. Future property damage from flooding: sensitivities to economy and climate change. Climatic Change 132, 741–749. https://doi.org/10.1007/s10584-015-1478-z.

Liu, Y.-F., Liu, Y., Shi, Z.-H., López-Vicente, M., Wu, G.-L., 2020a. Effectiveness of re-vegetated forest and grassland on soil erosion control in the semi-arid Loess Plateau. CATENA 195, 104787. https://doi.org/10.1016/j.catena.2020.104787.
Liu, S., Zhu, J., Yang, D., Ma, B., 2022. Comparative Study of Geological Hazard Evaluation Systems Using Grid Units and Slope Units under Different Rainfall Conditions. Sustainability 14, 16153. https://doi.org/10.3390/su142316153.
Long, S.-M., Li, G., 2021. Model Uncertainty in the Projected Indian Summer Monsoon Precipitation Change under Low-Emission Scenarios. Atmosphere 12, 248. https://doi.org/10.3390/atmos12020248.
Melillo, M., Brunetti, M.T., Peruccacci, S., Gariano, S.L., Guzzetti, F., 2015. An algorithm for the objective reconstruction of rainfall events responsible for landslides. Landslides 12, 311–320. https://doi.org/10.1007/s10346-014-0471-3.
Miao, C., Duan, Q., Sun, Q., Huang, Y., Kong, D., Yang, T., Ye, A., Di, Z., Gong, W., 2014. Assessment of CMIP5 climate models and projected temperature changes over Northern Eurasia. Environ. Res. Lett. 9, 055007 https://doi.org/10.1088/1748-9326/9/5/055007.
Mondal, S.K., Huang, J., Wang, Y., Su, B., Zhai, J., Tao, H., Wang, G., Fischer, T., Wen, S., Jiang, T., 2021. Doubling of the population exposed to drought over South Asia: CMIP6 multi-model-based analysis. Science of the Total Environment 771, 145186. https://doi.org/10.1016/j.scitotenv.2021.145186.
Murakami, D., Yamagata, Y., 2019. Estimation of Gridded Population and GDP Scenarios with Spatially Explicit Statistical Downscaling. Sustainability 11, 2106. https://doi.org/10.3390/su11072106.
Niu, X., Wang, S., Tang, J., Lee, D.-K., Gutowski, W., Dairaku, K., McGregor, J., Katzfey, J., Gao, X., Wu, J., Hong, S., Wang, Y., Sasaki, H., Fu, C., 2018. Ensemble evaluation and projection of climate extremes in China using RMIP models. Int. J. Climatol. 38, 2039–2055. https://doi.org/10.1002/joc.5315.
Noor, M., Ismail, T., Shahid, S., Nashwan, M.S., Ullah, S., 2019. Development of multi-model ensemble for projection of extreme rainfall events in Peninsular Malaysia. Hydrology Research 50, 1772–1788. https://doi.org/10.2166/nh.2019.097.
O'Neill, B.C., Tebaldi, C., van Vuuren, D.P., Eyring, V., Friedlingstein, P., Hurtt, G., Knutti, R., Kriegler, E., Lamarque, J.-F., Lowe, J., Meehl, G.A., Moss, R., Riahi, K., Sanderson, B.M., 2016. The Scenario Model Intercomparison Project (ScenarioMIP) for CMIP6. Geoscientific Model Development 9, 3461–3482. https://doi.org/10.5194/gmd-9-3461-2016.
Ortega, G., Arias, P.A., Villegas, J.C., Marquet, P.A., Nobre, P., 2021. Present-day and future climate over central and South America according to CMIP5/CMIP6 models. International Journal of Climatology 41, 6713–6735. https://doi.org/10.1002/joc.7221.
Pappenberger, F., Cloke, H.L., Parker, D.J., Wetterhall, F., Richardson, D.S., Thielen, J., 2015. The monetary benefit of early flood warnings in Europe. Environ. Sci. Policy 51, 278–291. https://doi.org/10.1016/j.envsci.2015.04.016.
Qin, P., 2022. More than six billion people encountering more exposure to extremes with 1.5 °C and 2.0 °C warming. Atmospheric Research 273, 106165. https://doi.org/10.1016/j.atmosres.2022.106165.
Ragettli, S., Tong, X., Zhang, G., Wang, H., Zhang, P., Stähli, M., 2019. Climate change impacts on summer flood frequencies in two mountainous catchments in China and Switzerland. Hydrology Research 52, 4–25. https://doi.org/10.2166/nh.2019.118.
Santer, B.D., Mears, C., Wentz, F.J., Taylor, K.E., Gleckler, P.J., Wigley, T.M.L., Barnett, T.P., Boyle, J.S., Brüggemann, W., Gillett, N.P., Klein, S.A., Meehl, G.A., Nozawa, T., Pierce, D.W., Stott, P.A., Washington, W.M., Wehner, M.F., 2007. Identification of human-induced changes in atmospheric moisture content. Proc. Natl. Acad. Sci. 104, 15248–15253. https://doi.org/10.1073/pnas.0702872104.
Shabariram, C.P., Kannammal, K.E., Manojpraphakar, T., 2016. Rainfall analysis and rainstorm prediction using MapReduce Framework, in: 2016 International Conference on Computer Communication and Informatics (ICCCI). Presented at the 2016 International Conference on Computer Communication and Informatics (ICCCI), pp. 1–4. https://doi.org/10.1109/ICCCI.2016.7479954.
Shi, X., Chen, J., Gu, L., Xu, C.-Y., Chen, H., Zhang, L., 2021. Impacts and socioeconomic exposures of global extreme precipitation events in 1.5 and 2.0 °C warmer climates. Science of the Total Environment 766, 142665. https://doi.org/10.1016/j.scitotenv.2020.142665.
Sillmann, J., Kharin, V.V., Zhang, X., Zwiers, F.W., Bronaugh, D., 2013. Climate extremes indices in the CMIP5 multimodel ensemble: Part 1. Model evaluation in the present climate. Journal of Geophysical Research: Atmospheres 118, 1716–1733. https://doi.org/10.1002/jgrd.50203.
Sonkoué, D., Monkam, D., Fotso-Nguemo, T.C., Yepdo, Z.D., Vondou, D.A., 2019. Evaluation and projected changes in daily rainfall characteristics over Central Africa based on a multi-model ensemble mean of CMIP5 simulations. Theor. Appl. Climatol. 137, 2167–2186. https://doi.org/10.1007/s00704-018-2729-5.
Srivastava, A., Grotjahn, R., Ullrich, P.A., 2020. Evaluation of historical CMIP6 model simulations of extreme precipitation over contiguous US regions. Weather Clim. Extremes 29, 100268. https://doi.org/10.1016/j.wace.2020.100268.
Sun, S., Dai, T.-L., Wang, Z.-Y., Chou, J.-M., Chao, Q.-C., Shi, P.-J., 2021. Projected increases in population exposure of daily climate extremes in eastern China by 2050. Advances in Climate Change Research 12, 804–813. https://doi.org/10.1016/j.accre.2021.09.014.
Ta, Z., Li, K., Han, H., Jin, Q., 2022. Population and GDP Exposure to Extreme Precipitation Events on Loess Plateau under the 1.5 °C Global Warming Level. Atmosphere 13, 1423. https://doi.org/10.3390/atmos13091423.
Takata, K., Hanasaki, N., 2020. The effects of afforestation as an adaptation option: a case study in the upper Chao Phraya River basin. Environ. Res. Lett. 15, 044020 https://doi.org/10.1088/1748-9326/ab7462.
Tan, M.L., Ibrahim, A.L., Duan, Z., Cracknell, A.P., Chaplot, V., 2015. Evaluation of Six High-Resolution Satellite and Ground-Based Precipitation Products over Malaysia. Remote Sensing 7, 1504–1528. https://doi.org/10.3390/rs70201504.
Tang, K.H.D., 2019. Climate change in Malaysia: Trends, contributors, impacts, mitigation and adaptations. Sci Total Environ 650, 1858–1871. https://doi.org/10.1016/j.scitotenv.2018.09.316.
Tang, B., Hu, W., 2022. Significant Increase in Population Exposure to Extreme Precipitation in South China and Indochina in the Future. Sustainability 14, 5784. https://doi.org/10.3390/su14105784.
Tate, E., Rahman, M.A., Emrich, C.T., Sampson, C.C., 2021. Flood exposure and social vulnerability in the United States. Nat Hazards 106, 435–457. https://doi.org/10.1007/s11069-020-04470-2.
Tellman, B., Sullivan, J.A., Kuhn, C., Kettner, A.J., Doyle, C.S., Brakenridge, G.R., Erickson, T.A., Slayback, D.A., 2021. Satellite imaging reveals increased proportion of population exposed to floods. Nature 596, 80–86. https://doi.org/10.1038/s41586-021-03695-w.
Thrasher, B., Wang, W., Michaelis, A., Melton, F., Lee, T., Nemani, R., 2022. NASA Global Daily Downscaled Projections, CMIP6. Sci Data 9, 262. https://doi.org/10.1038/s41597-022-01393-4.
United Nations Office for Disaster Risk Reduction, 2019. Global Assessment Report on Disaster Risk Reduction 2019. United Nations Office for Disaster Risk Reduction; UNDRR: Geneva, Switzerland, pp. 137-157. https://doi.org/10.18356/f4ae4888-en.
Uranchimeg, S., Kwon, H.-H., Kim, B., Kim, T.-W., 2020. Changes in extreme rainfall and its implications for design rainfall using a Bayesian quantile regression approach. Hydrology Research 51, 699–719. https://doi.org/10.2166/nh.2020.003.
Wang, H., Gao, T., Xie, L., 2019. Extreme precipitation events during 1960–2011 for the Northwest China: space-time changes and possible causes. Theor Appl Climatol 137, 977–995. https://doi.org/10.1007/s00704-018-2645-8.
Wang, J., Li, X., Christakos, G., Liao, Y., Zhang, T., Gu, X., Zheng, X., 2010. Geographical Detectors-Based Health Risk Assessment and its Application in the Neural Tube Defects Study of the Heshun Region, China. International Journal of Geographical Information Science 24, 107–127. https://doi.org/10.1080/13658810802443457.
Wang, C., Ren, X., Li, Y., 2017. Analysis of extreme precipitation characteristics in low mountain areas based on three-dimensional copulas—taking Kuandian County as an example. Theor Appl Climatol 128, 169–179. https://doi.org/10.1007/s00704-015-1692-7.
Wang, J.-F., Zhang, T.-L., Fu, B.-J., 2016. A measure of spatial stratified heterogeneity. Ecological Indicators 67, 250–256. https://doi.org/10.1016/j.ecolind.2016.02.052.
Weaver, C.P., Moss, R.H., Ebi, K.L., Gleick, P.H., Stern, P.C., Tebaldi, C., Wilson, R.S., Arvai, J.L., 2017. Reframing climate change assessments around risk: recommendations for the US National Climate Assessment. Environ. Res. Lett. 12, 080201 https://doi.org/10.1088/1748-9326/aa7494.
Wei, Y., Sun, S., Liang, D., Jia, Z., 2022. Spatial–temporal variations of NDVI and its response to climate in China from 2001 to 2020. International Journal of Digital Earth 15, 1463–1484. https://doi.org/10.1080/17538947.2022.2116118.
World Meteorological Organization, 2012. Chapter 14; Observation of present and past weather; state of the ground. In Guide to Meteorological Instruments and Methods of Observation; WMO: Geneva, Switzerland; pp. I.14–19.
Wu, S.-J., Lien, H.-C., Chang, C.-H., 2010. Modeling risk analysis for forecasting peak discharge during flooding prevention and warning operation. Stoch. Env. Res. Risk a. 24, 1175–1191. https://doi.org/10.1007/s00477-010-0436-6.
Xie, W., Zhou, B., Han, Z., Xu, Y., 2022. Substantial increase in daytime-nighttime compound heat waves and associated population exposure in China projected by the CMIP6 multimodel ensemble. Environ. Res. Lett. 17, 045007 https://doi.org/10.1088/1748-9326/ac592d.
Xu, H., Chen, H., Wang, H., 2022a. Increased populations will be exposed to the dangerous precipitation extremes across China in the future. Frontiers in Earth Science 10.
Xu, H., Chen, H., Wang, H., 2022b. Future changes in precipitation extremes across China based on CMIP6 models. Intl Journal of Climatology 42, 635–651. https://doi.org/10.1002/joc.7264.
Xu, C., Yuan, C., Li, X., Lin, Y., Fan, H., 2023. Projection of disaster-causing risk of extreme precipitation in the Yangtze River Basin based on CMIP6. Hydrol. Res. 54, 401–417. https://doi.org/10.2166/nh.2023.141.
Yang, Y., Cheng, S., Ren, Z., Li, Z., Jia, L., 2024. Operational Risk Assessment of Check Dams in Ningxia Considering the Impact of Extreme Precipitation in the Future. Water 16, 258. https://doi.org/10.3390/w16020258.
Zappa, G., Shepherd, T.G., 2017. Storylines of Atmospheric Circulation Change for European Regional Climate Impact Assessment. J. Climate 30, 6561–6577. https://doi.org/10.1175/JCLI-D-16-0807.1.
Zhang, Q., Li, J., Singh, V.P., Xiao, M., 2013. Spatio-temporal relations between temperature and precipitation regimes: Implications for temperature-induced changes in the hydrological cycle. Global and Planetary Change 111, 57–76. https://doi.org/10.1016/j.gloplacha.2013.08.012.
Zhang, M., Yang, X., Ren, L., Pan, M., Jiang, S., Liu, Y., Yuan, F., Fang, X., 2021. Simulation of Extreme Precipitation in Four Climate Regions in China by General Circulation Models (GCMs): Performance and Projections. Water 13, 1509. https://doi.org/10.3390/w13111509.
Zhao, J.-T., Su, B.-D., mondal, S.K., Wang, Y.-J., Tao, H., Jiang, T., 2021. Population exposure to precipitation extremes in the Indus River Basin at 1.5 °C, 2.0 °C and 3.0 °C warming levels. Advances in Climate Change Research 12, 199–209. https://doi.org/10.1016/j.accre.2021.03.005.
Zhao, F., Wu, Y., Yin, X., Sun, K., Ma, S., Zhang, S., Liu, S., Wang, W., Chen, J., 2022. Projected changes in population exposure to drought in China under CMIP6 forcing scenarios. Atmospheric Environment 282, 119162. https://doi.org/10.1016/j.atmosenv.2022.119162.
Zhou, T., Ren, L., Zhang, W., 2021. Anthropogenic influence on extreme Meiyu rainfall in 2020 and its future risk. Sci. China Earth Sci. 64, 1633–1644. https://doi.org/10.1007/s11430-020-9771-8.

Zhu, Z., Dai, Z., Li, S., Feng, Y., 2022. Spatiotemporal Evolution of Non-Grain Production of Cultivated Land and Its Underlying Factors in China. International Journal of Environmental Research and Public Health 19, 8210. https://doi.org/10.3390/ijerph19138210.

Zhu, H., Jiang, Z., Li, J., Li, W., Sun, C., Li, L., 2020. Does CMIP6 Inspire More Confidence in Simulating Climate Extremes over China? Adv. Atmos. Sci. 37, 1119–1132. https://doi.org/10.1007/s00376-020-9289-1.

Zhu, X., Xu, K., Liu, Y., Guo, R., Chen, L., 2021. Assessing the vulnerability and risk of maize to drought in China based on the AquaCrop model. Agricultural Systems 189, 103040. https://doi.org/10.1016/j.agsy.2020.103040.